

RESEARCH

Open Access



# Laboratory tests to understand tephra sliding behaviour on roofs

Sara Osman<sup>1\*</sup>, Mark Thomas<sup>1</sup>, Julia Crummy<sup>2</sup>, Anna Sharp<sup>1</sup> and Steve Carver<sup>3</sup>

## Abstract

Following explosive eruptions, loading from tephra fall deposits can lead to roof collapse. However, the load may be reduced significantly by tephra sliding on pitched roofs. We present small-scale laboratory tests to investigate tephra sliding behaviour on metal, fibre cement sheet and tile roofing. We tested 10–30 cm thicknesses for dry and wet deposits of pumice, scoria and basaltic ash. We found that tephra did not slide on roof pitches  $\leq 15^\circ$  for coarse-grained deposits and  $\leq 12^\circ$  for dry ash. Thin deposits of wet ash were stable at pitches  $\leq 30^\circ$ . In addition, tephra was mainly shed on pitches  $\geq 32^\circ$  for metal roofs and  $\geq 35^\circ$  for fibre cement and tiles. Using these results, we have produced an initial set of sliding coefficients for tephra for simply pitched roofs that can be used to help prioritise roofs for clearing during an eruption and assist in designing roofs to withstand tephra fall.

**Keywords** Ash fall, Roof loading, Building damage, Volcanic hazards, Eruption impacts

## Introduction

Tephra is the most widespread volcanic hazard, impacting large numbers of people and causing disruption across many sectors including infrastructure, agriculture and transport (e.g. Wilson et al. 2014; Jenkins et al. 2015). Buildings and building support systems can be damaged by even small amounts of tephra fall ( $\leq 10$  mm thick) if heating, ventilation and air-conditioning equipment is clogged by ash (Wilson et al. 2014) or leachates lead to corrosion of metal roofs over the longer term (Miller et al. 2022; Oze et al. 2014). Thicknesses of 10–100 mm may cause collapse of structures which are not built to regulated building design standards (non-engineered buildings) or which are in poor condition (Hayes et al.

2019a; Jenkins et al. 2014), as we observed on La Palma, Canary Islands during the 2021 eruption of Cumbre Vieja. Thicker deposits can lead to more widespread failure of roofs when the load exceeds the strength of the roof material or the supporting structure (Jenkins et al. 2014; Hampton et al. 2015).

Clean-up operations can mitigate the likelihood of roof failure (Hayes et al. 2015) and an understanding of loads on individual buildings can enable those structures at highest risk to be prioritised. On flat roofs, the tephra load is likely to be similar to that of the deposit on the ground (unless the roof is particularly sheltered or windswept) but on pitched roofs some of the tephra can slide off, potentially reducing the load on the roof significantly; therefore, it is important to understand tephra sliding behaviour. Tephra loads also have the potential to increase if conditions are wet, with field and laboratory observations showing load increases of 30–45% when rain falls after deposition (Hayes et al. 2019a; Williams et al. 2021).

Surveys following eruptions indicate that roofs can collapse at tephra loads of  $\sim 1$ – $10$  kPa, equivalent to tephra thicknesses of  $\sim 10$  cm –  $1$  m depending on deposit density. Key factors in determining the collapse load are

\*Correspondence:

Sara Osman  
eesjo@leeds.ac.uk

<sup>1</sup> School of Earth and Environment, University of Leeds, Woodhouse, Leeds LS2 9JT, UK

<sup>2</sup> British Geological Survey, The Lyell Centre, Research Avenue South, Edinburgh EH14 4AP, UK

<sup>3</sup> School of Geography, University of Leeds, Woodhouse, Leeds LS2 9JT, UK



© The Author(s) 2023. **Open Access** This article is licensed under a Creative Commons Attribution 4.0 International License, which permits use, sharing, adaptation, distribution and reproduction in any medium or format, as long as you give appropriate credit to the original author(s) and the source, provide a link to the Creative Commons licence, and indicate if changes were made. The images or other third party material in this article are included in the article's Creative Commons licence, unless indicated otherwise in a credit line to the material. If material is not included in the article's Creative Commons licence and your intended use is not permitted by statutory regulation or exceeds the permitted use, you will need to obtain permission directly from the copyright holder. To view a copy of this licence, visit <http://creativecommons.org/licenses/by/4.0/>. The Creative Commons Public Domain Dedication waiver (<http://creativecommons.org/publicdomain/zero/1.0/>) applies to the data made available in this article, unless otherwise stated in a credit line to the data.

the roof material, quality of construction and condition of the building (Blong 2003; Hayes et al. 2019a; Jenkins et al. 2014; Williams et al. 2020). However, despite almost 60 million people living within 10 km of a volcano that has the potential to erupt (Freire et al. 2019), global building standards do not routinely consider tephra loading. The loads imposed by heavy snowfall are however considered in some standards (e.g. British Standards Institution 2009; International Standards Organization 2013) and the approach they take on snow loading can help when considering how to assess tephra loading during building design. The Eurocodes are a harmonised set of documents that cover the technical aspects of structural and fire design of buildings and the civil engineering of structures. Document BS EN 1991-1-3 from within the Eurocodes deals with snow loads and a characteristic value of the load on the ground is selected using decades of historical data (British Standards Institution 2009; Sanpaolesi et al. 1998). This is then multiplied by a shape coefficient ( $\mu$ ), which takes account of sliding, to produce the load on the roof. Snow sliding behaviour depends mainly on temperature and altitude, and  $\mu$  values are defined by empirical equations based on roof load data (Sanpaolesi et al. 1999).

For consideration of tephra loads, this approach needs to be amended as large historical datasets for tephra fall do not exist. It is difficult to collect field data proximal to source, given the obvious hazard during the eruption

and the speed at which tephra deposits may subsequently be compacted or modified by wind and rain (e.g. Del Bello et al. 2021; Hayes et al. 2019b; Varekamp et al. 1984). Characteristic tephra ground loads for different eruption scenarios can be estimated using probabilistic tephra dispersion models (e.g. Barker et al. 2019; Vázquez et al. 2019; Wild et al. 2019), while tephra sliding behaviour depends on the density and thickness of the deposit and the roof material (Fig. 1, amended from Osman et al. 2022). Bulk (i.e. whole deposit) density varies with tephra type i.e. pumice, scoria or ash (which impacts grain density), the grain size distribution (which impacts deposit packing) and the amount of water in the deposit. To quantify how tephra sliding reduces roof load, we have carried out a series of laboratory tests to identify the roof pitches at which tephra loads are reduced or completely removed by sliding and have investigated how tephra type, grain size distribution, water content, deposit thickness and roof material influenced the angle of sliding (Fig. 1). From our results we have produced an indicative set of sliding coefficients for tephra loading as a first step to help assess the technical impact of tephra loading on simply pitched buildings in volcanic environments.

**Methods**

We carried out over 400 small-scale tilt table experiments to investigate sliding of pumice, scoria and basaltic ash in dry and wet conditions. We tested three roof

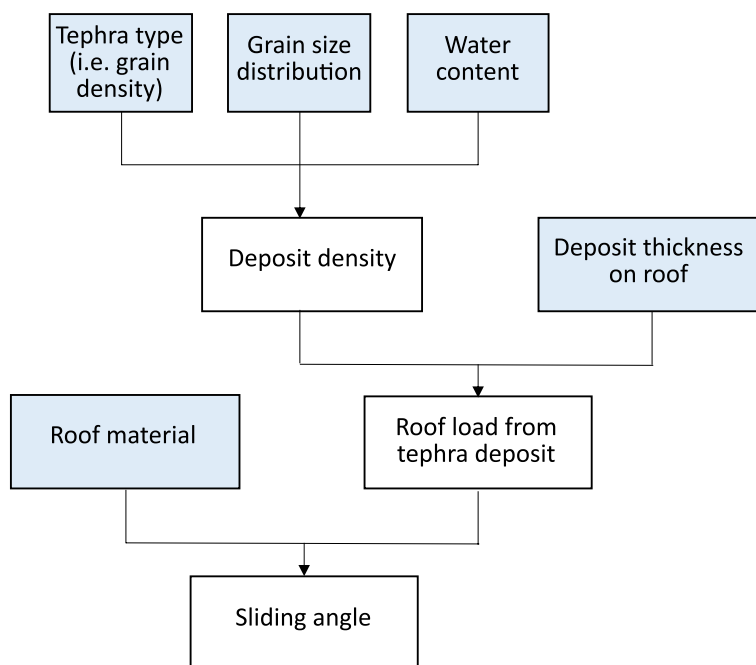


**Fig. 1** Key factors affecting sliding angle of tephra on roofs (amended from Osman et al. 2022). Shaded boxes represent the factors investigated in this study

materials: metal sheet (galvanized steel, 3" corrugated profile), fibre cement sheet (corrugated Eternit Profile 3 (Eternit 2021)) and clay tiles (Terreal Rustique plain tile (Terreal n.d.)). Tephra was loaded into Perspex cells with dimensions 22×22×10 cm (Fig. 2). The cells could move freely over each other, facilitated by the application of PTFE tape ("TEFSIL 3" from Techbelt Ltd, with coefficient of friction  $\leq 0.10$ ) between the cells to reduce friction. This ensured that sliding could occur both within the deposit and at the interface between the deposit and the roof material. We used one, two and three cells to observe sliding for tephra thicknesses of 10, 20 and 30 cm, respectively. Sliding tests were conducted with dry tephra on a dry roof (dry-dry), dry tephra on a wet roof (dry-wet) and wet tephra on a wet roof (wet-wet). Consideration of the impact the cell had on sliding is presented in a later section.

### Tephra samples

Large volumes of material were needed for the sliding tests, therefore synthetic tephra was used, created by crushing and grading commercially available volcanic aggregates of mafic and silicic composition. This material has been shown to be well matched to natural samples when considering the properties that are likely to affect sliding behaviour: bulk density, grain size distribution and internal angle of friction (Osman et al.

2022). To investigate the influence of grain size distribution and bulk density on sliding behaviour, we used three tephra samples (detailed in Fig. 3; Table 1): low density, coarse-to-fine grain size distribution (GSD) (pumice); high density, coarse-to-fine GSD (scoria) and high density, fine GSD (ash). We wanted to consider sliding from uniformly applied loads and hence minimise any affect from individual large clasts and we therefore selected a maximum grain size of  $-4 \phi$  (16 mm). This maximum grain size is also consistent with samples used to assess the geomechanical properties of tephra (Osman et al. 2022), where the size of the apparatus used to conduct the geomechanical tests limits the maximum size of individual particles relative to the total sample size.

We tested both wet and dry tephra. For the wet samples we aimed to simulate tephra that was naturally saturated by rainfall, adding the maximum amount of water to the sample and stopping as soon as any runoff from the sample occurred. The dry tephra sample was weighed and placed on a board inclined at  $5^\circ$ , to allow excess water to drain. Water was added gradually so that the finest grains were not washed out, and the sample was then mixed thoroughly to ensure it was uniformly wet. When water was observed draining from the sample it was left to fully drain off any excess water and then reweighed. The water content was calculated by:

$$\text{Water content (weight \%)} = \frac{(\text{wet weight of tephra} - \text{dry weight of tephra}) * 100}{\text{dry weight of tephra}}$$

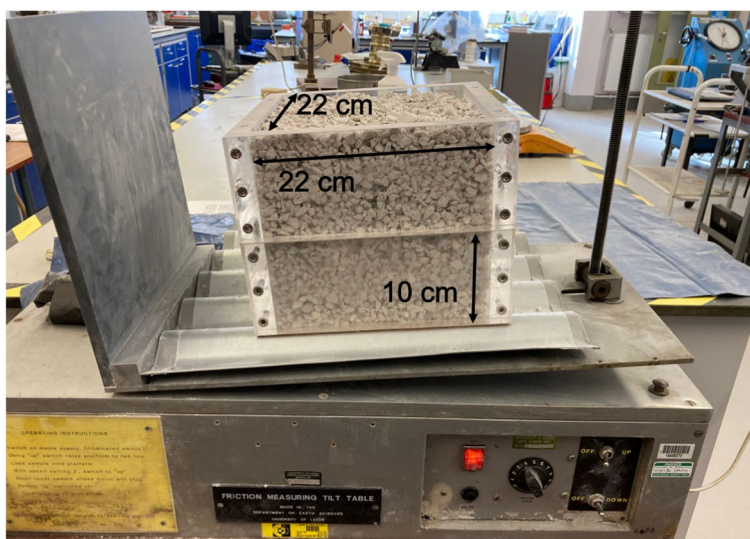


**Fig. 2** Tilt table set-up. The roof material was placed on the horizontal tilt table, the cell was placed on it and filled with tephra. The inclination of the table was then increased in half degree increments until tephra sliding occurred

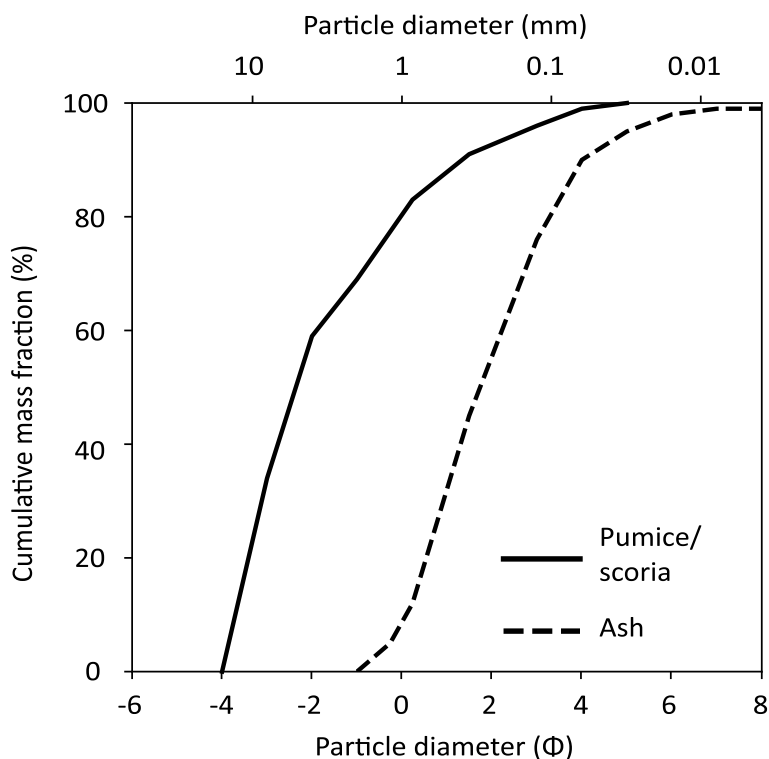


**Fig. 3** Grain size distribution for pumice, scoria and ash used in sliding tests

**Table 1** Grain size, deposit density and equivalent tephra loads for pumice, scoria and ash test samples

Tephra type	Wet/Dry	Median grain size		Maximum grain size		Mean deposit density (kg m <sup>-3</sup> )	Equivalent distributed tephra load (kPa) for test deposit thickness		
		(φ)	(mm)	(φ)	(mm)		10 cm	20 cm	30 cm
Pumice	Dry	-2.3	5	-4	16	433	0.42	0.85	1.27
Pumice	Wet	-2.3	5	-4	16	556	0.55	1.09	1.64
Scoria	Dry	-2.3	5	-4	16	1235	1.21	2.42	3.63
Scoria	Wet	-2.3	5	-4	16	1152	1.13	2.26	3.39
Ash	Dry	1.7	0.3	-1	2	1443	1.41	2.83	4.24
Ash	Wet	1.7	0.3	-1	2	1574	1.54	3.09	4.63

The recorded water contents for pumice, scoria and ash were 40 wt%, 15 wt% and 22 wt% respectively, which were then used in all “wet” sliding tests for these materials.

The mean bulk densities of the dry samples ranged from 433 to 1443 kg m<sup>-3</sup> (Table 1). These values are within published deposit density values of ~400–1500 kg m<sup>-3</sup>, covering a wide range of eruption sizes and compositions (Osman et al. 2022). However, when loaded into the test cell, wet sample bulk deposit density did not increase as much as expected based on theoretical literature values (Macedonio and Costa 2012).

In the dry deposits, any finer particles were free to move relative to the larger grains, filling void spaces. When wet, the fine particles aggregated around and adhered to larger grains, leading to less efficient deposit packing and more void space. This resulted in the bulk density of wet pumice increasing by 28%, while the bulk density of wet scoria actually decreased by 7% compared to the dry samples. For ash, the dry deposit flowed like a powder but when wet, it did not flow at all and density changes between - 6% and +10%, with respect to the dry density, were possible. To better constrain the wet

ash bulk density, we used a value consistent with field samples of basaltic ash and lapilli collected during the La Palma 2021 eruption. For these samples, collected within a few days of deposition and following rain, the natural deposit density was measured as ~10% higher than the sample’s dry density (after oven drying). We therefore aimed to replicate this for all our wet ash tests (Table 1).

For the coarser deposits, we investigated whether pouring tephra into the load cell from a greater height (forcing greater compaction) would increase the bulk density and whether this would impact the sliding angle. We poured tephra into the load cell directly and from a height of ~1.5 m when particles ≤1 mm diameter would reach terminal velocity (Bagheri and Bonadonna 2016). Deposit density increased for the samples poured from height (from ~500 to 600 kg m<sup>-3</sup> for pumice and from ~1000 to 1200 kg m<sup>-3</sup> for scoria) but the sliding angle did not change. We therefore ensured deposit density was within these ranges for all our sliding tests with wet pumice and scoria (Table 1).

**Initial sliding tests**

We conducted a series of tests to ensure that sliding was controlled by the tephra and not the Perspex cell, including consideration of the weight of the cell and its

placement over the ridges (rather than the troughs) of the corrugated sheets.

**Control of sliding**

We conducted sliding tests with an empty cell to identify the minimum angle at which sliding would be controlled by the tephra. The edges of the empty cell were coated in PTFE tape (“TEFSIL 3’ from Techbelt Ltd, with coefficient of friction ≤0.10) to reduce friction (Fig. 4a). The cell was placed on each roof material and the roof angle increased until sliding occurred (Fig. 4b). Sliding angles are shown in Table 2. For the tiles, the sliding angle was >30° which is similar to the expected internal angle of friction for tephra deposits (Osman et al. 2022), and so the PTFE tape was also applied to the tile directly beneath the cell.

**Effect of corrugations**

For the corrugated metal and fibre cement sheets, tests with 10 cm thickness of pumice were carried out with the cell edges over the troughs and the ridges of the roofing sheet to check whether the direct contact of the ridges along the entire down-slope length of the cell impacted the sliding angle. When the cell edges were over the ridges, little tephra leakage occurred. When



**Fig. 4** Initial test set-up, **a** Perspex cell with edges coated in PTFE tape, **b** testing the sliding angle for one empty Perspex cell on metal sheet, **c** testing the sliding angle using a cardboard cell

**Table 2** Sliding angles for the empty Perspex cell on all roof materials used in the sliding tests and for the Perspex cell with 10 cm thickness of pumice on the corrugated sheets. For corrugated sheets, angles were measured with the cell placed over the ridges and over the troughs. In each case, 3 tests were performed

Roofing material	Cell over ridge or trough	Mean empty cell sliding angle (°)	Mean sliding angle (°) with 10 cm thickness of pumice
Fibre cement	Ridge	24	32
Fibre cement	Trough	21	32
Metal sheet	Ridge	19	26
Metal sheet	Trough	13	27
Tile (no PTFE tape)	N/A	32	
Tile (with PTFE tape)	N/A	24	

the edges were over the troughs, the weight of tephra held the deposit in place with tephra only leaking as we started to fill the cell and when it slid along the roof material. No measurable difference was found in the sliding angle (Table 2) and so for all the remaining tests the cell was placed over the ridges, as this minimised tephra loss when sliding occurred.

**Effect of cell weight**

To investigate whether the presence of the Perspex cell or the area of the cell in contact with the roofing material affected the sliding angle, we carried out tests using a cardboard cell weighing < 50 g, with the cell walls being ~ 0.3 cm thick (Fig. 4c). We tested 10 and 20 cm of pumice on all roof materials using the cardboard cell. The only notable observed difference between the Perspex cell (of weight 2.35 kg for each 10 cm depth) and the cardboard cell was that on tiles with 20 cm thickness of pumice, the tephra “leaked” from beneath the sides of the cell before sliding occurred. No measurable difference was seen between the sliding angles for tests using the cardboard and Perspex cells (Fig. 5).

Despite the significant difference in material, weight and cell wall size, changing from one cell type to the other had no effect on the recorded sliding angles and as a result of these tests, we are confident that it is the tephra that is controlling the sliding rather than any of the test equipment. The tests and results discussed in this

manuscript therefore assume that all sliding behaviour is controlled by the tephra.

**Angle of repose and initial movement of tephra grains**

The repose angle of the deposit and initial movement of the grains (rolling and sliding on the surface of the deposit) were investigated with the tilt table set horizontally, by gently pouring tephra to approximately half fill one side of the cell. The repose angle was measured, and the table was then raised in half degree increments until the grains on the surface of the deposit started to move. In some tests, individual grains rolled at low tilt angles, but the initial movement angle was measured when grains moved across a substantial part of the deposit surface. By investigating when the deposit starts to move with only one half of the cell filled, we are able to account for the fact that the deposit is completely contained in the cell during the sliding tests, and mitigate any possibility that the initial recorded onset of sliding would be inhibited by the cell.

**Sliding tests**

With the tilt table set horizontally, the roof material and then the load cell were added (Fig. 2). The tephra sample was weighed, and tephra was carefully poured into the cell and distributed to ensure that the deposit was evenly dispersed into the corners of the cell. After the cell was filled, the remaining tephra was weighed and the

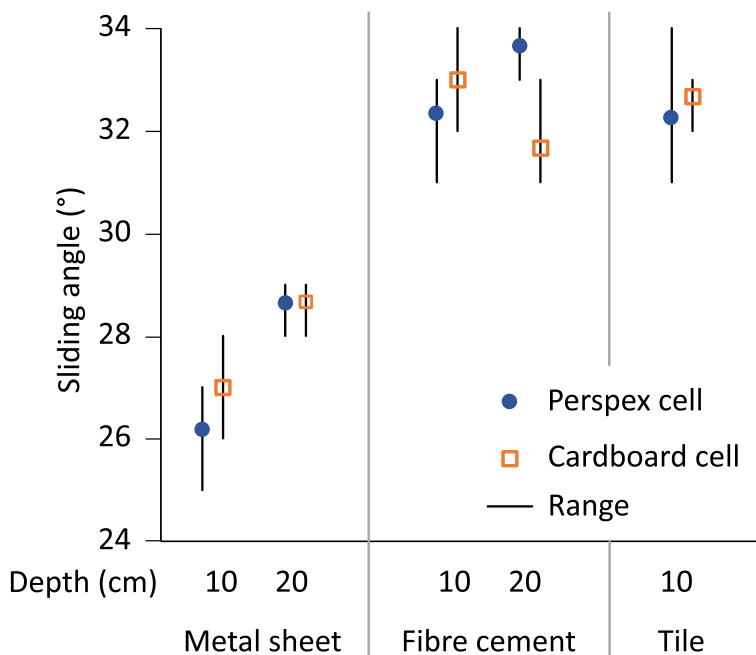


**Fig. 5** Comparison of sliding angles for cardboard and Perspex cells with 10 and 20 cm thickness of pumice on metal sheet, fibre cement and tiles

mass of test tephra in the cell was calculated. This mass was kept constant throughout the series of tests. The volume of tephra was calculated from measurements of the dimensions of the cell (plus an estimate of the volume of the corrugations for the metal and fibre cement sheets) and from this the bulk density of the test deposit was calculated (Table 1). Tephra loads for the tests ranged from 0.42 kPa for 10 cm of dry pumice to 4.63 kPa for 30 cm of wet ash (Table 1).

To ensure the motion of the tilt table did not initiate sliding, slope angle was increased slowly in half degree increments until sliding occurred, when the angle of tilt was measured with a clinometer. Tests were replicated five times, apart from 10 cm of pumice on the corrugated roof sheets, where 6 tests were carried out (3 with the cell over the ridges and 3 over the troughs).

For the dry-wet and wet-wet tests, the tilt table was set to 5°, the empty load cell was added, and the roof was thoroughly wetted ensuring the whole area within the cell was wet. Any excess water was allowed to run off and tephra was then immediately poured onto the roofing before the surface dried.

The effect of roof condition was also investigated by testing 20 cm of both pumice and scoria on a very weathered (moss-covered) fibre cement sheet and a weathered metal sheet. Both sheets, supplied by Garage Revamps (<http://www.revamps.co.uk>), had been on garage roofs in the UK for >10 years. The weathered fibre cement tests

were only able to be carried out twice, as the surface in contact with the tephra was substantially changed after each test due to the sliding deposit scouring the moss and material that had built up on the surface of the roof.

**Results**

**Angle of repose and initial movement of the grains**

The mean angle of repose was the same for all dry deposits (35°), with a range of 33–36° for pumice and 34–37° for scoria and ash (Fig. 6). For the wet deposit, the mean repose angle increased to 48° for pumice, 43° for scoria and 42° for ash.

In dry samples, grains initially started rolling and sliding over each other at tilt angles of 10–14° for ash (mean: 12°) and 13–16° for the coarser-grained samples (mean: 14° for pumice and 15° for scoria). No change was seen when scoria was wetted, but wet pumice grains required a higher tilt before movement started (mean value 18°), as shown in Fig. 6. Wet ash behaved very differently to the dry sample, with apparent cohesion between the grains resulting in more stable deposits. The 10 cm deposit failed by sliding at the base at a tilt angle of 28° on metal sheet, and slumping at a tilt of 30° on fibre cement and tile, and slumping at a tilt of 21°.

**Sliding tests**

Mean sliding angles varied between 26° and 33° for pumice, 24° and 36° for scoria and 23° and 36° for ash (range

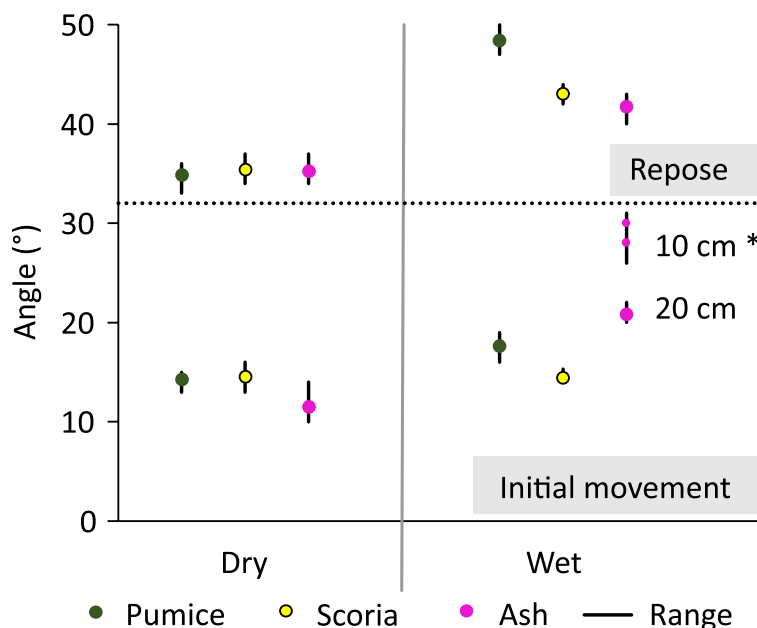


**Fig. 6** Repose angle and angle at which tephra grains started to move on the surface of the deposit for dry and wet pumice, scoria and ash. \* Initial movement of wet ash varied with deposit thickness. 10 cm: sliding at the base (between tephra and roof) at 28° on metal sheet and slumping of deposit at 30° on fibre cement and tile; 20 cm: slumping at 21°

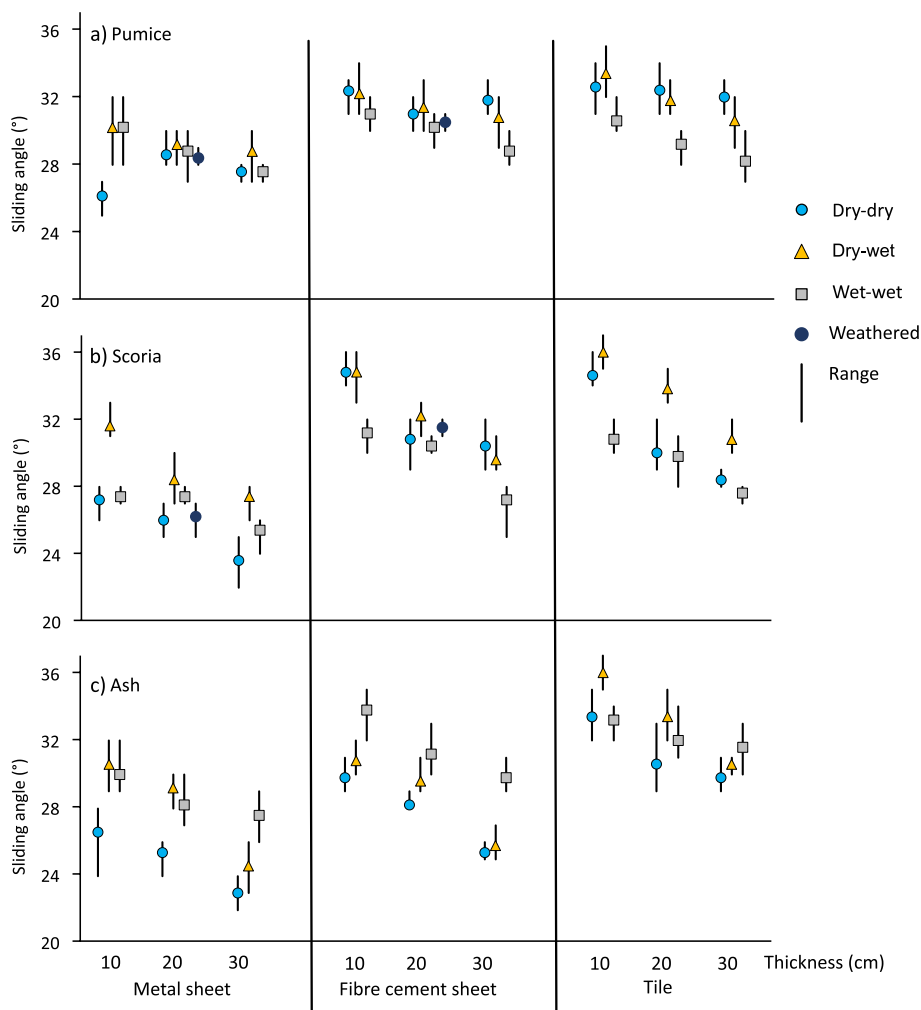


**Fig. 7** Mean sliding angles and range of values for tilt tests with 10–30 cm of pumice, scoria and ash on metal sheet, fibre cement and tile roofing. Dry deposits were tested on dry and wet roofs; wet deposits were tested on wet roofs. Dry deposits of 10 and 20 cm of pumice and scoria were also tested on dry weathered metal and fibre cement. In the key the hyphenated symbol descriptions refer to the state (dry or wet) of the deposit-roof. All results are available in [Supplementary material](#)

for total dataset: 22–37°) (Fig. 7). Deposits slid at shallower angles on metal sheet compared to fibre cement and tiles (Fig. 8), and at shallower angles on each roof material when the deposit was thicker (Fig. 8a). There were no clear trends when considering grain size (Fig. 8b) but on fibre cement and tile, the steepest sliding angles for pumice were lower than for scoria and ash (Fig. 8c).

When considering the impact of water, for the low friction metal sheet the dry-dry tests resulted in the shallowest sliding angle for all tephra types and the dry-wet test typically gave the steepest sliding angle (Figs. 7 and 8d). When the roof was wet, the tephra in contact with the metal sheet formed a distinct layer that appeared to hold the deposit at steeper roof angles. On fibre cement and tiles, results varied with tephra type

(Fig. 7). For fibre cement, the steepest sliding angles were for the dry-dry and dry-wet tests for the coarse-grained deposits and the wet-wet tests for ash. On tiles, the dry-dry and dry-wet tests gave the steepest sliding angles for pumice, the dry-wet tests for scoria and the dry-wet and wet-wet tests for ash. Sliding angles on weathered metal and fibre cement sheet fell within the range found for new roofing sheets for both pumice and scoria deposits (Fig. 7).

For the dry, coarser-grained tephra, sliding always occurred at the base of the deposit, that is at the interface of the deposit and the roofing material, except for one test with 30 cm of pumice on fibre cement, where sliding occurred within the deposit. For dry ash, sliding always occurred at the base on the metal sheet and fibre



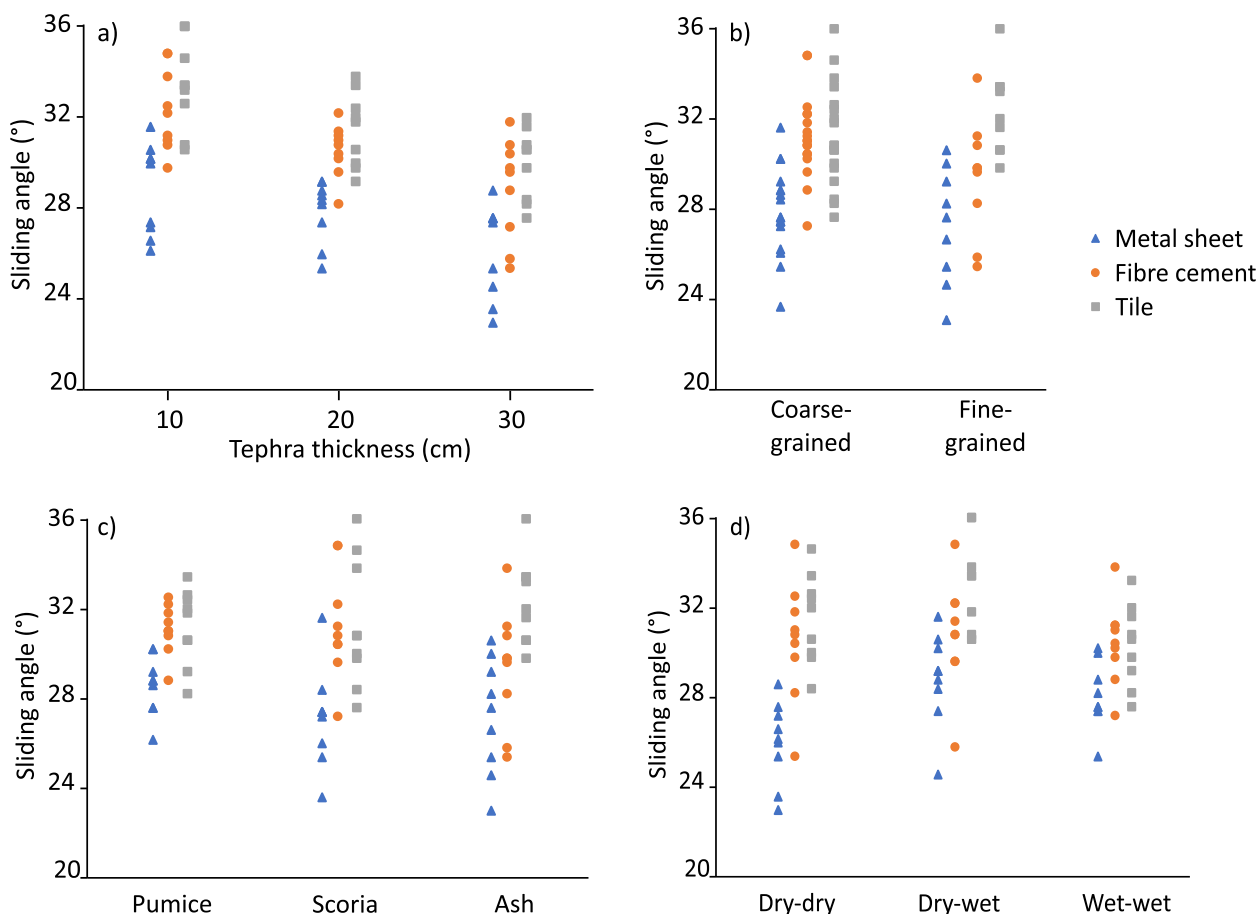


**Fig. 8** Impact of key factors (shown in Fig. 1) on mean sliding angles for tilt tests, **a** deposit thickness: 10, 20 30 cm, **b** grain size: coarse-grained, fine-grained (defined in Fig. 3), **c** tephra type: pumice, scoria, ash, **d** presence of water: dry tephra on dry roof, dry tephra on wet roof, wet tephra on wet roof. Plots show results on three roof materials: metal sheet, fibre cement sheet and tiles

**Table 3** Number of sliding tests (of 5 in total in each case) where failure occurred through sliding within the tephra rather than at the base of the deposit. For all other tests, sliding occurred between the tephra and the roofing material

Test	Tephra thickness	
	20 cm	30 cm
Dry-dry	Ash: 2 on tile	Pumice: 1 on fibre cement Ash: 5 on tile
Dry-wet	Ash: 3 on tile	Ash: 5 on tile
Wet-wet		Pumice: 3 on fibre cement; 4 on tile Scoria: 1 on fibre cement; 5 on tile Ash: 2 on fibre cement; 1 on tile

cement. On tiles, approximately half of the dry-dry and dry-wet tests failed within the tephra at 20 cm thickness, and all failed within the tephra for the 30 cm thick deposit (Table 3). For wet tephra, 20 cm thick deposits

always slid at the base, but at 30 cm thickness, sliding was observed both at the base and within the tephra (Table 3). Thicker deposits failed more often by overcoming the internal friction between the grains rather than the friction between the tephra and the roofing material. For ash this mechanism was more likely when the deposit was dry, while for the coarser-grained samples it mainly occurred in wet deposits.

**Discussion**

When assessing whether roofs are likely to collapse under tephra loading, we need to consider how much, if any, of a tephra deposit will slide off and so reduce the load. Our experiments considered low- and high-density tephra, coarse and fine grain size distributions, both dry and wet, at thicknesses up to 30 cm on metal, fibre cement and tile roofing. These results can therefore provide initial bounds on when sliding is likely to occur for a range of deposits and roof materials for simply pitched roofs.

**Angle of repose and initial movement of grains**

Our mean repose angle of 35° for dry tephra is consistent with the internal angle of friction of 35.8–36.5° observed in shear box tests for dry samples with the same grain size distributions (Osman et al. 2022). Published experimental results of 35° for ash and 40–45° for coarse tephra (Hornby et al. 2020; Williams et al. 2021) seem to suggest that the finer grains in our sample are controlling the repose angle. Mean repose angles of 42–48° for wet deposits are consistent with findings for other granular materials that water increases the repose angle (e.g. Hornbaker et al. 1997; Beakawi Al-Hashemi and Baghabra Al-Amoudi 2018).

The angle at which grains initially move gives an indication of the shallowest roof pitch where sliding might occur. Our values of ~15° for the coarser-grained deposits and ~12° for dry ash are consistent with experiments simulating ash deposition on metal roofing, which found 26% of the ash was shed from a 15° roof (Hampton et al.

2015). The behaviour of wet ash, where a 10 cm deposit could be stable to ~30° and a 20 cm deposit slumped at ~21°, requires further investigation on larger scale roofs and at greater tephra thickness than possible with our equipment. However, overall, our results suggest that low pitched roofs can be considered as flat when assessing how sliding may reduce tephra loading, consistent with our observations in La Palma, Canary Islands, following the 2021 Cumbre Vieja eruption (Fig. 9).

**Sliding**

The angle at which the entire test deposit slid gives an indication of the shallowest roof pitch on which most of the deposit will be shed. For steeper angles than those recorded we expect the load to be entirely removed as we have assumed that the tephra is not inhibited from sliding off the roof by the presence of guttering or snow guards. Roof collapse occurs when the tephra load exceeds the roof failure load. Even without sliding, our



**Fig. 9** Low pitched roofs in (a) Las Manchas and (b) Tacande, La Palma following the Cumbre Vieja 2021 eruption, showing no evidence of the deposit sliding except at the deposit edges where the angle of repose has been formed

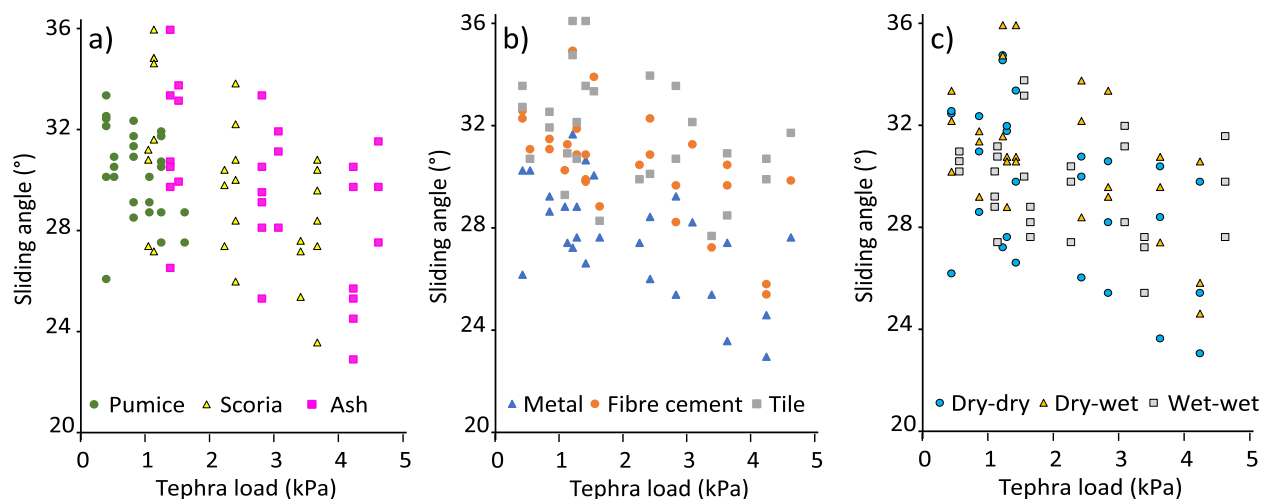


**Fig. 10** Summary plot showing variation of mean sliding angle with tephra load for all tests, highlighted by a tephra type, b roof material and c presence of water

maximum tested pumice test loads of  $<2$  kPa (Fig. 10a) are unlikely to lead to collapse unless roofs are of poor quality or badly maintained (Jenkins et al. 2014). However, test loads of 1–4 kPa and 1–5 kPa for scoria and ash respectively could lead to collapse in good quality buildings, hence sliding is an important factor to consider. As expected, our results show that sliding occurs at a shallower angle on the lower friction metal sheet compared to the rougher surfaces of fibre cement and tiles (Fig. 10b). When considering the other factors we investigated (shown in Fig. 1), namely deposit thickness, tephra type, grain size distribution and presence of water, there is a clear trend on each roof type for the sliding angle to be lower for higher loads (i.e. thicker deposits) (Fig. 10), but no clear trends related to the other factors (Fig. 10a, c). This suggests the increased weight of tephra is key in overcoming the frictional forces that resist sliding when compared to other factors.

We found that metal roofs require a pitch  $\geq 32^\circ$  to ensure the deposit is substantially shed, consistent with larger scale tests using dry basaltic ash, where  $\sim 45\%$  of the deposit remained on a  $30^\circ$  metal sheet roof, reducing to  $<10\%$  at  $35^\circ$  (Hampton et al. 2015). For fibre cement and tiles, a pitch of  $\geq 35^\circ$  is needed to significantly shed tephra, which is consistent with our observations of tile roofs in La Palma, where sliding had occurred on a pitch  $\sim 35^\circ$  but tephra built up on a  $\sim 20^\circ$  section (Fig. 11).

The impact of rainfall on deposit behaviour likely depends on whether it occurs before, during or after tephra deposition. Our “wet” tests aimed to simulate tephra falling during rain as the tephra was wet before

deposition into the test cells. Our measured wet density increases of 28% for pumice and 9% for ash are consistent with observations following the eruption of Pinatubo in 1991 (Spence et al. 2005) and our findings on La Palma in 2021, respectively. However, for wet scoria, as our bulk density was 7% lower than for the dry deposit, higher saturated loads may be possible if deposition from the plume leads to more efficient grain packing than achieved in our tests. For rain falling after deposition, grain size distribution and rainfall intensity affect the depth to which water can penetrate and hence its impact on sliding (Tarasenko et al. 2019; Williams et al. 2021). Our maximum sliding angle for wet tephra ( $36^\circ$  for both scoria and ash) is substantially lower than previous results where wet ash remained stable at  $45^\circ$  pitch (Hampton et al. 2015). These higher values, taken with our observations that wet ash deposits demonstrated apparent cohesion, suggest that further work, including at large scale, is particularly needed to investigate the behaviour of fine-grained tephra when water is present.

In our tests, sliding mainly occurred at the base of the tephra, between the deposit and the roof material. However, on the higher friction roofing material, and in particular for thicker deposits and when water was present, sliding also occurred within the deposit (Table 3). This suggests that for these roofs and for thicker, wetter tephra deposits, the failure mechanism depends on the internal angle of friction of the tephra rather than the type of roofing material and that the frictional strength at the deposit–roof interface in these situations is higher than the internal frictional strength of the tephra deposit.



**Fig. 11** Tephra deposit on a roof in Tacande, La Palma, December 2021 during the Cumbre Vieja eruption. Tephra has slid on the steeper part of the roof ( $\sim 35^\circ$  pitch) but accumulated on the lower, shallower part ( $\sim 20^\circ$ )

### Implications for disaster risk management

Disaster risk considers the potential harms to people and infrastructure in a community resulting from their exposure to a hazard, mitigated by their capacity to deal with its impacts (United Nations Office for Disaster Risk Reduction 2016). Understanding when tephra fall loads might lead to building collapse and how deposit sliding may reduce that risk can help when assessing priorities for clean-up during and after an eruption and when planning for future eruptions.

For buildings proximal to the source, clearing roofs of tephra can significantly reduce the risk of building failure, but clean-up operations often pose significant logistical and health and safety challenges (Hayes et al. 2015; IVHHN 2021). Our results can help prioritise roofs for clearance by highlighting when the deposit is likely to be reduced by sliding. We found that pumice and scoria deposits are unlikely to slide on roofs with pitches  $\leq \sim 15^\circ$  while for fine-grained tephra, roofs  $\leq \sim 12^\circ$  can be treated as flat. In addition, much of the load is likely to be shed on metal roofs with pitches  $\geq 32^\circ$  and fibre cement or tile roofs with pitches  $\geq 35^\circ$ .

We also found that weathering of the roof material did not significantly change tephra sliding behaviour, although when considering the physical load that a roof can withstand, it would be important to consider any deterioration in the material strength due to environmental exposure which might result in collapse at lower imposed loads. Of course, the roofing material may not be the weakest part of the roof and collapse may occur through failure of weak structural support, as was observed following the Cordón Caulle 2011 eruption (Elissondo et al. 2016) and most recently in La Palma after the 2021 eruptions (e.g. Dominguez Barragan et al. 2022). Surveys of roofs on both engineered and non-engineered buildings around Galeras volcano in Columbia estimated that collapse after tephra fall could occur under loads of 0.5–5 kPa, with the roof support structure and the type and quality of roofing material being key factors in determining failure load (Torres-Corredor et al. 2017). A range of failure points were also identified following the Pinatubo 1991, Rabaul 1994 and Kelud 2014 eruptions (roof covering, rafters and purlins), with longer span roofs and those with overhangs performing poorly (Blong 2003; Spence et al. 2005; Williams et al. 2020).

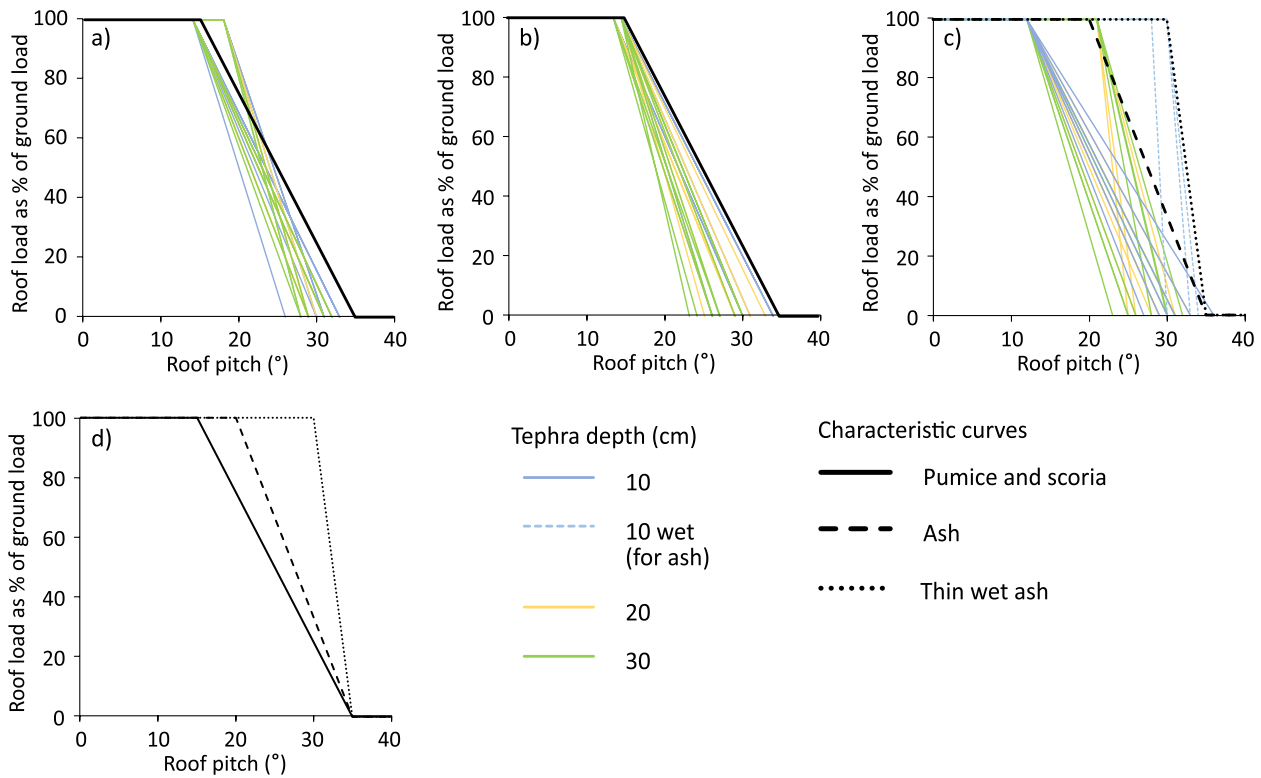
Over the longer term, the risk of failure in vulnerable areas could be reduced by planning buildings with pitches  $\geq 35^\circ$  to enhance the likelihood of tephra sliding. Existing buildings where tephra is unlikely to slide could also be identified and roof strengthening considered for particular key buildings (e.g. Zuccaro and Leone 2012).

### Implications for building design

Building design standards aim to ensure that buildings remain fit for purpose during their design life and take account of transient loads such as snow (e.g. British Standards Institution 2009; International Standards Organization 2013). Although tephra loads are not routinely considered, the snow load approach could be adapted for tephra loading. The Eurocode standard for snow loading (BS EN 1991-3) first defines a characteristic value for snow load on the ground, taken as the load with an expected 50-year return period (British Standards Institution 2009). This value is calculated using an empirical equation which was derived from statistical analyses of historical snow depth measurements and takes account of local climatic conditions (Sanpaolesi et al. 1998). The ground load is then multiplied by a shape coefficient (ranging from 0 to 1) which accounts for the fraction of the load that slides off a roof depending on its shape. These shape coefficients were derived from measurements of ground and roof snow loads collected for 81 buildings over the 1998-99 winter season (Sanpaolesi et al. 1999).

For tephra loading, the characteristic value of the ground load could routinely be obtained from numerical modelling of different eruption scenarios (e.g. Barker et al. 2019; Vázquez et al. 2019; Wild et al. 2019). To build up a comprehensive set of sliding coefficients tephra sliding behaviour must be quantified on a wide range of roof shapes and materials. As a first step towards this, our results can inform values for simply pitched roofs. By making the following assumptions, we can summarise all our results to show how the fraction of ground load remaining on a roof varies with roof pitch for the different tephra types we considered (Fig. 12a-c):

- The angle at which grains initially move (Fig. 6) represents the lowest roof pitch at which any tephra load is likely to be removed by sliding.
- The deposit sliding angle (Fig. 7) represents the steepest pitch on which any ash will remain.
- Load reduces linearly for roofs with pitches between these values.
- Initial sliding occurs at the same angle in 20 and 30 cm deposits (as we were unable to measure this for 30 cm thickness with our equipment).
- Where tephra deposits slide internally rather than at the interface with the roofing material, this action results in the erosion of the underlying deposit so that there is little difference between deposits that fail at the base or internally.

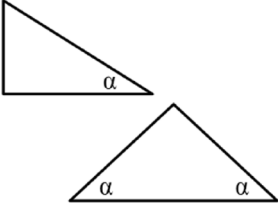


**Fig. 12** Summary of all tests showing percentage of ground tephra load expected to remain on a roof for deposits of (a) pumice, (b) scoria, (c) ash. Characteristic values for each tephra type are shown in (d). Load is assumed to reduce linearly for roof pitches between lab values for initial movement and total sliding

We can then select characteristic curves for each tephra type (Fig. 12d). In building design, it is usual to present results with a 95% confidence interval, but the number of tests needed for that is beyond the scope of this study due to the limited size of the test equipment and roofing materials available to test. We have however

selected conservative values and, for this initial assessment, chosen changes of slope at 5° intervals (i.e. at 15, 20, 30 and 35°). Pumice and scoria can be represented by a single curve (Fig. 12a,b), while ash requires two curves (Fig. 12c): one for thin, wet deposits, which are stable at steep roof pitches, and one for all other ash.

**Table 4** Tephra sliding coefficients for monopitch and simply pitched roofs

Roof type	Tephra type	Low pitch	Medium pitch	Steep pitch	Equation
	Coarse-grained (Pumice or scoria)	$\alpha \leq 15^\circ$ $\mu_{\text{coarse}} = 1$	$15^\circ < \alpha < 35^\circ$ $\mu_{\text{coarse}} = (35 - \alpha)/20$	$35^\circ \leq \alpha$ $\mu_{\text{coarse}} = 0$	(1)
	Fine-grained (Ash)	$\alpha \leq 20^\circ$ $\mu_{\text{fine}} = 1$	$20^\circ < \alpha < 35^\circ$ $\mu_{\text{fine}} = (35 - \alpha)/15$	$35^\circ \leq \alpha$ $\mu_{\text{fine}} = 0$	(2)
	Wet ash < 20 cm thick <sup>a</sup>	$\alpha \leq 30^\circ$ $\mu_{\text{finewet}} = 1$	$30^\circ < \alpha < 35^\circ$ $\mu_{\text{finewet}} = (35 - \alpha)/5$	$35^\circ \leq \alpha$ $\mu_{\text{finewet}} = 0$	(3)

<sup>a</sup> When considering critical roof loads, this case will likely only lead to failure for dense deposits or low strength roofs

As a final step, we can present these results as indicative sliding coefficient equations for simply pitched roofs (Table 4), using the same format as the Eurocode snow loading coefficients. The sliding coefficient,  $\mu$ , varies with roof pitch and is a multiplier that converts tephra load on the ground to tephra load on a roof. The geological setting is important when considering likely deposit characteristics in any future eruption, and expert judgement of local hazard should be used to select the most appropriate Eqs. (1, 2 or 3) in any area.

#### Limitations and future work

When considering building failure due to natural hazards, there will ultimately be the possibility of loss. For financial loss, insurance companies typically use vulnerability curves to link hazard intensity (in our case, tephra fall loads) to likely damage for different building types (Blong et al. 2017; Oramas-Dorta et al. 2021). Exposure is often considered at a regional scale, aligning with information held by insurers, as exposure data at the level of individual buildings are rarely available (Murnane et al. 2019; Silva et al. 2018). However, where detailed asset information is obtained, we see the potential of using our results to shift the vulnerability curves depending on tephra type and roof shape, providing more accurate damage and loss estimates for tephra fall events. In the case of loss of life, the best approach to avoid this is to identify the hazard and reduce the risk. The hazard posed by tephra loading leading to roof collapse is obvious, but the risk is controlled by the quality of the structure and ability of the tephra load to be shed. The characteristic curves developed here demonstrate the process through which this risk can begin to be calculated.

To fully realise the potential benefits of this work more testing on different materials and at different scales is needed. The findings presented here relate to uniform loads on simply pitched roofs and assume that the tephra load is removed when the deposit slides, rather than being redistributed on the roof. Our experiments do not represent the process of deposition, where the deposit may be stratified by grain size (Eychenne and Engwell 2022) and tephra falls on an inclined surface, while in our tests we poured tephra onto a horizontal surface which was then inclined. The rate of deposition may also affect the ability of tephra to slide or be cleared, clogging of gutters may form barriers inhibiting sliding (Hampton et al. 2015) and for multi-pitched roofs, sliding from one area may lead to increased loading elsewhere. We have not considered post-depositional changes, where rain can lead to deposit surfaces becoming cemented, which may affect the sliding behaviour (Tarasenko et al. 2019). Wind can also cause drifting on sheltered roofs and this can significantly increase loading, as has been seen from field

observations and laboratory tests for snow loads (e.g. Bennett et al. 2014; Wang et al. 2020; Zhang et al. 2021).

We have focused on one of the hazards of tephra fall, namely increased roof loading. However, fire from hot tephra and impact from larger ballistics should also be considered (e.g. Hampton et al. 2015; Williams et al. 2019). In addition, if the deposit remains in place long term, corrosion may weaken metal roofs, as was reported in Montserrat (Sword-Daniels et al. 2014) and Rabaul, Papua New Guinea (Blong 2003), although laboratory tests indicate this is unlikely to occur over timescales less than one month (Oze et al. 2014). It would be useful to investigate how tephra fall may promote corrosion and lead to building failures beyond proximal areas, considering both the residue left after sliding (as we found in our dry-wet tests) and deposits thinner than 10 cm. We have also not considered any structural aspects of roofs, but these are important when assessing the collapse risk for individual roofs (Torres-Corredor et al. 2017).

The largest limitation of our work is that our tests were small-scale and considered sliding on a simple slope for three roof materials. The volumes of tephra required for large-scale testing precluded statistically relevant testing on even just three roofing materials within the scope of this project, and the importance of testing the influence of different roofing materials was considered a priority. Larger scale experiments are however now needed to confirm our results and assess the impact of the roof structure on failure. Tests covering other roof materials and more complex roof geometries would also add to these findings and allow application to a wider range of roof types found in areas at risk of tephra loading.

In contrast to our other tephra samples, wet ash did not flow and thin deposits were stable to high angles (30° on fibre cement and tiles) before failing by slumping or sliding along the roof. This means that our assumption that roof loads decrease linearly for roofs with pitches between the initial movement and final sliding angles (Fig. 12) may not be valid for this deposit. Again, larger scale tests should investigate how varying thicknesses of wet ash behave on different roof materials and slopes.

#### Conclusions

Using small-scale laboratory tests to investigate tephra sliding behaviour on roofs, we have developed a set of preliminary sliding coefficients for monopitched or simply pitched roofs. These have been derived by adapting the European Eurocode standard procedure for snow loads on roofs. Our tests considered thicknesses of 10, 20 and 30 cm on corrugated metal, fibre cement sheets and tiles for dry and wet deposits of low-density pumice and high-density scoria with a coarse-to-fine grain size

distribution (median grain size =  $-2.3 \phi$  (5 mm)), as well as high density basaltic ash (median grain size =  $1.7 \phi$  (0.3 mm)).

Our results show that sliding of coarse-grained deposits is unlikely to occur on roofs with pitches  $\leq 15^\circ$ , while for dry ash this value is  $\sim 12^\circ$ . Wet ash behaved differently with thin deposits (10 cm thick) stable at pitches up to  $30^\circ$ ; however, our results for wet ash are inconclusive and further work is needed to investigate the effects of water on ash deposits. In addition, the load is mainly shed on metal roofs with pitches  $\geq 32^\circ$  and fibre cement or tiles with pitches  $\geq 35^\circ$ , values that hold for both new and weathered roofing.

For monopitch and simply pitched roofs, we have produced characteristic curves and sliding coefficients enabling tephra loads on a roof to be estimated from the ground load. These results can assist in prioritising roofs to be cleared during and after an eruption. This is a first step towards developing building standards for tephra loading; however, there is further work to be done. Additional roof types need consideration to build up a comprehensive set of sliding coefficients that can be used in building design and large, structure-scale testing is required to validate the laboratory results.

## Supplementary Information

The online version contains supplementary material available at <https://doi.org/10.1186/s13617-023-00137-2>.

**Additional file 1: Supplementary material.** Sliding test results.

## Acknowledgements

Thanks to Kirk Handley, University of Leeds for assistance with the lab equipment, to Tony Windross and Stephen Burgess, University of Leeds for customising the tilt table and constructing the sliding cells and to Garage Revamps for providing the weathered roof materials. Thanks also to two anonymous reviewers whose constructive comments helped us to improve the manuscript.

## Authors' contributions

The project was devised by MT and JC and supervised by MT, JC and SC. SO undertook laboratory work and data analysis. AS contributed to laboratory work. SO wrote the manuscript with inputs from MT, JC, AS and SC. All authors read and approved the final manuscript.

## Funding

SO is supported by the Leeds-York-Hull Natural Environment Research Council (NERC) Doctoral Training Partnership (DTP) Panorama under grant NE/S007458/1. This work was in part funded by the British Geological Survey University Funding Initiative (BUFI) PhD studentship S426. JC publishes with permission of the executive director of the British Geological Survey (UKRI).

## Availability of data and materials

All sliding test results are available as [Supplementary material](#).

## Declarations

## Ethics approval and consent to participate

Not applicable.

## Competing interests

The authors declare no competing interests.

Received: 28 April 2023 Accepted: 16 October 2023

Published online: 06 November 2023

## References

- Bagheri G, Bonadonna C (2016) Aerodynamics of volcanic particles: characterization of size, shape, and settling velocity. In: Mackie S, Cashman K, Ricketts H, Rust A, Watson M (eds) *Volcanic ash: hazard observation*. Elsevier, pp 39–52. <https://doi.org/10.1016/B978-0-08-100405-0.00005-7>
- Barker SJ, Van Eaton AR, Mastin LG, Wilson CJN, Thompson MA, Wilson TM, Davis C et al (2019) Modeling ash dispersal from future eruptions of Taupo Supervolcano. *Geochem Geophys Geosyst* 20(7):3375–3401. <https://doi.org/10.1029/2018GC008152>
- Beakawi Al-Hashemi HM, Baghabra Al-Amoudi OS (2018) A review on the angle of repose of granular materials. *Powder Technol* 330:397–417. <https://doi.org/10.1016/j.powtec.2018.02.003>
- Bennett PJ, Peterka JA, Harris JR (2014) A case study in drifting snow behavior. In: *Proceedings of the 2014 Structures Congress*. American Society of Civil Engineers, pp 34–45. <https://doi.org/10.1061/9780784413357.004>
- Blong R (2003) Building damage in Rabaul, Papua New Guinea, 1994. *Bull Volcanol* 65(1):43–54. <https://doi.org/10.1007/s00445-002-0238-x>
- Blong RJ, Grasso P, Jenkins SF, Magill CR, Wilson TM, McMullan K et al (2017) Estimating building vulnerability to volcanic ash fall for insurance and other purposes. *J Appl Volcanology* 6:2. <https://doi.org/10.1186/s13617-017-0054-9>
- British Standards Institution (2009) BS EN 1991-1-3: 2003 + A1:2015. Eurocode 1 – actions on structures. Part 1–3: general actions – snow loads. BSI, London
- Del Bello E, Taddeucci J, Merrison JP, Rasmussen KR, Andronico D, Ricci T et al (2021) Field-based measurements of volcanic ash resuspension by wind. *Earth Planet Sci Lett* 554:116684. <https://doi.org/10.1016/j.epsl.2020.116684>
- Dominguez Barragan L, Di Maio L, Reyes Hardy M-P, Frischknecht C, Zuccaro G, Perez N, Bonadonna C (2022) Impact assessment of buildings exposed to the tephra fallout of the 2021 Cumbre Vieja eruption in La Palma, Spain. *EGU General Assembly 2022*, Vienna, Austria, 23–27 May 2022, EGU22-12678. <https://doi.org/10.5194/egusphere-egu22-12678>
- Eliasson M, Baumann V, Bonadonna C, Pistolesi M, Cioni R, Bertagnini A, Biass S et al (2016) Chronology and impact of the 2011 Cordón Caulle eruption, Chile. *Nat Hazards Earth Syst Sci* 16(3):675–704. <https://doi.org/10.5194/nhess-16-675-2016>
- Eternit (2021) Profiled sheeting: description, properties and performance. Technical note Et-01/08/en/v1. <https://www.eternit.co.uk/-/dam/eternit-material-information-data-sheet/pd17895/original/eternit-material-information-data-sheet.pdf>. Accessed: 28 Jan 2022
- Eychenne J, Engwell SL (2022) The grain size of volcanic fall deposits: spatial trends and physical controls. *GSA Bull* 135(7–8):1844–1858. <https://doi.org/10.1130/B36275.1>
- Freire S, Florczyk AJ, Pesaresi M, Sliuzas R (2019) An improved global analysis of population distribution in proximity to active volcanoes, 1975–2015. *ISPRS Int J Geo-Information* 8:341. <https://doi.org/10.3390/ijgi8080341>
- Hampton SJ, Cole JW, Wilson G, Wilson TM, Broom S (2015) Volcanic ashfall accumulation and loading on gutters and pitched roofs from laboratory empirical experiments: implications for risk assessment. *J Volcanol Geoth Res* 304:237–252. <https://doi.org/10.1016/j.jvolgeores.2015.08.012>
- Hayes JL, Wilson TM, Magill C (2015) Tephra fall clean-up in urban environments. *J Volcanol Geoth Res* 304:359–377. <https://doi.org/10.1016/j.jvolgeores.2015.09.014>
- Hayes JL, Calderón R, Deline NI, Jenkins SF, Leonard GS, Mcsporrán AM, Williams GT et al (2019) Timber-framed building damage from tephra fall and lahar: 2015 Calbuco eruption, Chile. *J Volcanol Geoth Res* 374:142–159. <https://doi.org/10.1016/j.jvolgeores.2019.02.017>
- Hayes JL, Wilson TM, Stewart C, Villarosa G, Salgado P, Beigt D et al (2019) Tephra clean-up after the 2015 eruption of Calbuco volcano, Chile: a quantitative geospatial assessment in four communities. *J Appl Volcanology* 8:7. <https://doi.org/10.1186/s13617-019-0087-3>

- Hornbaker DJ, Albert R, Albert I, Barabasi AL, Schiffer P (1997) What keeps sandcastles standing? *Nature* 387:765. <https://doi.org/10.1038/42831>
- Hornby AJ, Kueppers U, Maurer B, Poetsch C, Dingwell DB (2020) Experimental constraints on volcanic ash generation and clast morphometrics in pyroclastic density currents and granular flows. *Volcanica* 3(2):263–283. <https://doi.org/10.30909/VOL.03.02.263283>
- International Standards Organization (2013) ISO 4355:2013. Bases for design of structures — determination of snow loads on roofs. ISO, Geneva
- IVHHN (2021) Health and safety considerations for ashfall clean-up: briefing note. [https://www.ivhhn.org/uploads/IVHHN\\_briefing\\_note\\_clean-up\\_health\\_safety.pdf](https://www.ivhhn.org/uploads/IVHHN_briefing_note_clean-up_health_safety.pdf). Accessed: 28 Mar 2023
- Jenkins SF, Spence RJS, Fonseca JFBD, Solidum RU, Wilson TM (2014) Volcanic risk assessment: quantifying physical vulnerability in the built environment. *J Volcanol Geoth Res* 276:105–120. <https://doi.org/10.1016/j.jvolgeoes.2014.03.002>
- Jenkins SF, Wilson T, Magill C, Miller V, Stewart C, Blong R, Marzocchi W et al (2015) Volcanic ash fall hazard and risk. In: Loughlin SC, Sparks RSJ, Brown SK, Jenkins SF, Vye-Brown C (eds) *Global volcanic hazards and risk*. Cambridge University Press, pp 173–221. <https://doi.org/10.1017/CBO9781316276273.005>
- Macedonio G, Costa A (2012) Brief communication: rain effect on the load of tephra deposits. *Nat Hazards Earth Syst Sci* 12(4):1229–1233. <https://doi.org/10.5194/nhess-12-1229-2012>
- Miller VL, Joseph EP, Sapkota N, Szarzynski J (2022) Challenges and opportunities for risk management of volcanic hazards in small-island developing states. *Mt Res Dev* 42(2):D22–D31. <https://doi.org/10.1659/MRD-JOURNAL-D-22-00001.1>
- Murnane RJ, Allegri G, Bushi A, Dabbeek J, de Moel H, Duncan M et al (2019) Data schemas for multiple hazards, exposure and vulnerability. *Disaster Prev Manage* 28(6):752–763. <https://doi.org/10.1108/DPM-09-2019-0293>
- Oramas-Dorta D, Tirabassi G, Franco G, Magill C (2021) Design of parametric risk transfer solutions for Volcanic Eruptions: an application to Japanese volcanoes. *Nat Hazards Earth Syst Sci* 21(1):99–113. <https://doi.org/10.5194/nhess-21-99-2021>
- Osman S, Thomas M, Crummy J, Carver S (2022) Investigation of geometrical properties of tephra relevant to roof loading for application in vulnerability analyses. *J Appl Volcanology* 11:9. <https://doi.org/10.1186/s13617-022-00121-2>
- Oze C, Cole J, Scott A, Wilson T, Wilson G, Gaw S, Hampton S et al (2014) Corrosion of metal roof materials related to volcanic ash interactions. *Nat Hazards* 71(1):785–802. <https://doi.org/10.1007/s11069-013-0943-0>
- Sanpaulesi L, Currie D, Sims P, Sacré C, Stieffel U, Lozza S, Eisel B et al (1998) Scientific support activity in the field of structural stability of civil engineering works: snow loads. Final report phase I. Commission of the European Communities DGIII/D-3, Brussels. <https://www2.ing.unipi.it/dic/snowloads/Final%20Report%20I.pdf>. Accessed 30 Sept 2022
- Sanpaulesi L, Brettell M, Currie D, Dillon P, Sims P, Delpech P, Duffresne M et al (1999) Scientific support activity in the field of structural stability of civil engineering works: snow loads. Final report phase II. Commission of the European Communities DGIII/D-3, Brussels. <https://www2.ing.unipi.it/dic/snowloads/Final%20Report%20II.pdf>. Accessed 30 Sept 2022
- Silva V, Yepes-Estrada C, Dabbeek J, Martins L, Brzev S (2018) GED4ALL – global exposure database for multi-hazard risk analysis – multi-hazard exposure taxonomy, GEM Technical Report 2018-01. Pavia, Italy: GEM Foundation. [http://www.gfdrr.org/sites/default/files/publication/Exposure%20data%20schema\\_final%20report.pdf](http://www.gfdrr.org/sites/default/files/publication/Exposure%20data%20schema_final%20report.pdf). Accessed 30 Sept 2023
- Spence RJS, Kelman I, Baxter PJ, Zuccaro G, Petrazzuoli S (2005) Residential building and occupant vulnerability to tephra fall. *Nat Hazards Earth Syst Sci* 5(5):477–494. <https://doi.org/10.5194/nhess-5-477-2005>
- Sword-Daniels V, Wilson TM, Sargeant S, Rossetto T, Twigg J, Johnston DM, Loughlin SC et al (2014) Consequences of long-term volcanic activity for essential services in Montserrat: challenges, adaptations and resilience. In: *The Eruption of Soufrière Hills Volcano, Montserrat from 2000 to 2010*. Wadge G, Robertson REA, Voight, B (eds). Geological Society, London, 471–488. <https://doi.org/10.1114/M39.26>
- Tarasenko I, Biolders CL, Guevara A, Delmelle P (2019) Surface crusting of volcanic ash deposits under simulated rainfall. *Bull Volcanol* 81:30. <https://doi.org/10.1007/S00445-019-1289-6>
- Terreal (n.d.) Roofing book. [https://terreal.co.uk/fileadmin/UK/4\\_Downloads/TERREAL-RoofingBook.pdf](https://terreal.co.uk/fileadmin/UK/4_Downloads/TERREAL-RoofingBook.pdf). Accessed 31 Jan 2022
- Torres-Corredor RA, Ponce-Villarreal P, Gómez-Martínez DM (2017) Vulnerabilidad física de cubiertas de edificaciones de uso de ocupación normal ante caídas de ceniza en la zona de influencia del Volcán Galeras. *Boletín de Geología* 39(2):67–82. <https://doi.org/10.18273/revbol.v39n2-2017005>
- United Nations Office for Disaster Risk Reduction (2016) Report of the open-ended Intergovernmental Expert Working Group on indicators and terminology relating to disaster risk reduction. New York: UNDRR. <https://www.undrr.org/publication/report-open-ended-intergovernmental-expert-working-group-indicators-and-terminology>. Accessed 04 July 2023
- Varekamp JC, Luhr JF, Prestegard KL (1984) The 1982 eruptions of El Chichón Volcano (Chiapas, Mexico): character of the eruptions, ash-fall deposits, and gasphase. *J Volcanol Geoth Res* 23(1–2):39–68. [https://doi.org/10.1016/0377-0273\(84\)90056-8](https://doi.org/10.1016/0377-0273(84)90056-8)
- Vázquez R, Bonasia R, Folch A, Arce JL, Macías JL (2019) Tephra fallout hazard assessment at Tacaná volcano (Mexico). *J S Am Earth Sci* 91:253–259. <https://doi.org/10.1016/j.jsames.2019.02.013>
- Wang J, Liu H, Chen Z, Ma K (2020) Wind tunnel test of wind-induced snow-drift on stepped flat roofs during snowfall. *Nat Hazards* 104:731–752. <https://doi.org/10.1007/s11069-020-04188-1>
- Wild AJ, Wilson TM, Bebbington MS, Cole JW, Craig HM (2019) Probabilistic volcanic impact assessment and cost-benefit analysis on network infrastructure for secondary evacuation of farm livestock: a case study from the dairy industry, Taranaki, New Zealand. *J Volcanol Geoth Res* 387:106670. <https://doi.org/10.1016/j.jvolgeoes.2019.106670>
- Williams GT, Kennedy BM, Lallemand D, Wilson TM, Allen N, Scott A, Jenkins SF (2019) Tephra cushioning of ballistic impacts: quantifying building vulnerability through pneumatic cannon experiments and multiple fragility curve fitting approaches. *J Volcanol Geoth Res* 388:106711. <https://doi.org/10.1016/j.jvolgeoes.2019.106711>
- Williams GT, Jenkins SF, Biass S, Wibowo HE, Harijoko A (2020) Remotely assessing tephra fall building damage and vulnerability: Kelud Volcano, Indonesia. *J Appl Volcanology* 9:10. <https://doi.org/10.1186/s13617-020-00100-5>
- Williams GT, Jenkins SF, Lee DWJ, Wee SJ (2021) How rainfall influences tephra fall loading - an experimental approach. *Bull Volcanol* 83:42. <https://doi.org/10.1007/s00445-021-01465-0>
- Wilson G, Wilson TM, Deligne NI, Cole JW (2014) Volcanic hazard impacts to critical infrastructure: a review. *J Volcanol Geoth Res* 286:148–182. <https://doi.org/10.1016/j.jvolgeoes.2014.08.030>
- Zhang G, Zhang Q, Fan F, Shen S (2021) Field measurements of snowdrift characteristics on reduced scale building roofs based on the size effect study. *Structures* 32:2020–2031. <https://doi.org/10.1016/j.jistruc.2021.04.002>
- Zuccaro G, Leone MF (2012) Building technologies for the mitigation of volcanic risk: Vesuvius and Campi Flegrei. *Nat Hazards Rev* 13(3):221–232. [https://doi.org/10.1061/\(ASCE\)NH.1527-6996.0000071](https://doi.org/10.1061/(ASCE)NH.1527-6996.0000071)

## Publisher's Note

Springer Nature remains neutral with regard to jurisdictional claims in published maps and institutional affiliations.

Ready to submit your research? Choose BMC and benefit from:

- fast, convenient online submission
- thorough peer review by experienced researchers in your field
- rapid publication on acceptance
- support for research data, including large and complex data types
- gold Open Access which fosters wider collaboration and increased citations
- maximum visibility for your research: over 100M website views per year

At BMC, research is always in progress.

Learn more [biomedcentral.com/submissions](https://biomedcentral.com/submissions)

